JOURNAL OF AIRCRAFT
Vol. 39, No. 5, September–October 2002

Velocity Field Above a Rotor Disk by a New Dynamic Inflow Model

Jorge A. Morillo* and David A. Peters†
Washington University, St. Louis, Missouri 63130

The potential flow equations are converted to ordinary differential equations through a Galerkin approach in which velocity and pressure potential functions are expanded in terms of closed-form solutions to Laplace's equation. Because the method gives differential equations for the flow in terms of a relatively few generalized coordinates that represent modes of the flowfield, the resultant equations can be used effectively in preliminary design, real-time simulations, and dynamic eigenvalue analysis for aeroelasticity. This new theory is more general than the Peters–He dynamic wake model because it has a more rigorous derivation and includes inflow modes previously neglected in the Peters–He model. Results are presented in the frequency domain for simple harmonic motion. The complete velocity field above the disk is obtained by this new methodology, for axial and skewed flows, for various skew angles, and for different pressure distributions and are compared with the Peters–He model and with an exact solution obtained by a convolution integral.

Nomenclature

A	=	area on the rotor disk plane ($z=0$) corresponding to the on-disk surface
$\boldsymbol{A}\cdot\boldsymbol{B}$	=	dot product of $\boldsymbol{A}$ and $\boldsymbol{B}$
a_n^m, $\hat{a}_n^m$	=	cosine-induced inflow expansion coefficients
B	=	area on the rotor disk plane ($z=0$) corresponding to the off-disk surface
b_n^m, $\hat{b}_n^m$	=	sine-induced inflow expansion coefficients
C	=	surface area of the upper-half volume at infinity
D_{jn}^{rm}	=	element of $[D]$
$[D]$	=	damping matrix
H_n^m	=	$[(n+m-1)!!(n-m-1)!!]/[(n+m)!!(n-m)!!]$
K_n^m	=	$(\pi/2)^{(-1)^{n+m}} H_n^m$
$\tilde{L}_{jn}^{rm}$	=	element of $[\tilde{L}]$
$[\tilde{L}]$	=	influence coefficient matrix
M_{jn}^{rm}	=	element of $[M]$
$[M]$	=	mass matrix
m, r	=	harmonic numbers
n, j	=	polynomial numbers
$(n)!!$	=	double factorial of n $(n)!!=(n)(n-2)(n-4),\ldots,(2)$, $n=$ even $(n)!!=(n)(n-2)(n-4),\ldots,(1)$, $n=$ odd $(0)!!=1$; $(-1)!!=1$; $(-2)!!=\infty$; $(-3)!!=-1$
P	=	pressure divided by $V_\infty^2\rho$ (nondimensional)
$\bar{P}_n^m(\nu)$	=	normalized Legendre function of first kind
p	=	pressure
$\bar{Q}_n^m(i\eta)$	=	normalized Legendre function of second kind
R	=	rotor radius
S	=	surface of integration, $A+B+C$
s	=	rotor disk plane ($z=0$), $A+B$
t	=	time
$\bar{t}$	=	nondimensional time, Ωt
V	=	volume of integration, corresponding to the upper-half volume of the inflow
V_∞	=	freestream velocity
$\boldsymbol{v}$	=	induced velocity vector divided by V_∞
$v_r, v_z, v_{\bar{\psi}}$	=	radial, axial, and aximuthal induced velocity components
x, y, z	=	nondimensional rotor disk coordinates, coordinate divided by R
$\Delta\dot{m}$	=	mass flow per unit area
δ_{nj}	=	Kronecker delta
$\bar{\eta}$	=	freestream velocity V_∞ divided by ΩR
Λ_j^{rc}, Λ_j^{rs}	=	cosine and sine parts of test potentials
$\nu, \eta, \bar{\psi}$	=	ellipsoidal coordinates
ξ	=	nondimensional coordinate along freestream line, positive upstream
ρ	=	air density
ς_n^m, σ_n^m	=	velocity potential expansion coefficients
τ	=	reduced time, that is, $\bar{\eta}\bar{t}\equiv V_\infty t/R=\tau$
τ_n^{mc}, τ_n^{ms}	=	cosine and sine parts of pressure coefficients
Φ_n^{mc}, Φ_n^{ms}	=	cosine and sine parts of pressure potentials
χ	=	wake skew angle
Ψ_n^{mc}, Ψ_n^{ms}	=	cosine and sine parts of velocity potentials
ω	=	reduced frequency
∇	=	Laplacean operator

Subscripts

$_e$	=	$n+m$ even
$_o$	=	$n+m$ odd

Superscripts

-1	=	matrix inverse
$*$	=	derivative with respect to reduced time, that is, $\partial/\partial\tau$

Introduction

PITT and Peters[1] used principles of potential flow theory to represent the axial component of the induced velocity at the rotor disk in terms of a finite number of inflow states. They obtained an unsteady flow model that gave excellent correlation with wind-tunnel response data throughout the frequency and advance ratio range. However, despite the unquestioned success of this Pitt–Peters inflow model, it has only three inflow degrees of freedom: 1) uniform, 2) fore to aft, and 3) side to side.

Received 8 June 2001; revision received 13 May 2002; accepted for publication 14 May 2002.

*Graduate Student and Boeing Fellow, Mechanical Engineering Department, Campus Box 1185.

†McDonnell Douglas Professor of Engineering and Chairman, Mechanical Engineering Department, Campus Box 1185. AIAA Fellow.

Later, Peters et al.[2] showed how the Pitt–Peters[1] ideas could be truly generalized to a theory with an arbitrary number of inflow harmonics and an arbitrary number of radial shape functions per harmonic. They[2] showed how the general theory could reduce in special cases to the old Pitt–Peters model[1] as well as to Loewy theory and Prandtl tip-loss theory. This new theory was used to correlate unsteady wind-tunnel data from the NASA Langley Research Center wind tunnel for various planforms, thrust coefficients, and advance ratios.[3] The match in both steady and unsteady distributions was excellent.

The Peters–He model[3] represents a mature dynamic inflow model that is now used in many production codes, including 2GCHAS (government code), FLIGHTLAB (Advanced Rotorcraft Technology), COPTER (Bell Helicopter), ONERA–DFVLR (European Community), and many university applications.

The inflow models described in the preceding paragraphs are formulated such that the states of the model represent induced flow distributions on the rotor disk (expanded radially as polynomials and azimuthally as Fourier coefficients). The first-order differential equations for these states depend on the freestream impingement angle, flight speed, and thrust level. However, they are all in closed form in terms of a mass matrix and a damping matrix, such that they are easily assembled either into a comprehensive code, an eigenvalue analysis, or a flight simulator. This makes the model extremely efficient.

However, in many of the applications, such as ground effect work,[4] it is necessary to find not just the normal flow at the disk, but all three components of flow off of the disk as well. Peters and Morillo[5] presented a consistent methodology for computing all three components of the flow in axial flow, both on and off of the rotor disk within the context of a finite state model. The model is formulated in a manner fairly similar to previous work (in that the potential functions in ellipsoidal coordinates are used). However, in contrast with the previous work, the states represent velocity potentials rather than individual flow components. In addition, all potential functions are considered (not just the ones that have a pressure discontinuity across the disk), and the derivation of the equation coefficients is done in a more consistent and rigorous manner than in the earlier derivations. The result is a simpler derivation and a more complete inflow theory for the velocity both off and on the disk. Previous dynamic inflow models in axial flow are shown to be special cases of the new model when off-disk coupling is neglected. This new methodology, based on a Galerkin approach, provides the exact solution on as well as off the disk for the axial velocity component in axial flow.

In this paper, the concepts introduced by Peters and Morillo[5] are extended to analyze skewed flow cases.

Fluid Dynamics Equations

The three-dimensional flow equations (momentum and continuity equations) for the pressure and velocity fields P and $\boldsymbol{v}$, with a freestream velocity V_∞, are

$$\frac{\partial \boldsymbol{v}}{\partial \tau} - \frac{\partial \boldsymbol{v}}{\partial \xi} = -\nabla P \tag{1}$$

$$\nabla \cdot \boldsymbol{v} = 0 \tag{2}$$

As with earlier inflow models, V_∞ can be generalized to include heavy lift and hover, but here it is treated as a constant.

Equations (1) and (2) have been nondimensionalized by defining P as pressure divided by ρV_∞^2, $\boldsymbol{v}$ as induced velocity divided by V_∞, and time as a reduced time τ, that is, time multiplied by V_∞/R. The variable ξ is the nondimensional coordinate along the freestream line, positive upstream. All lengths are divided by the rotor radius R. Figure 1 shows the coordinate system.

From continuity [Eq. (2)], it can be seen that, if $\boldsymbol{v}$ is represented by a gradient of some function Ψ, it is clear that Ψ will satisfy Laplace's equation. It can also be shown that P satisfies Laplace's equation. Therefore, P can be expressed as a summation of pressure potentials Φ, and $\boldsymbol{v}$ can be expressed as a summation of the gradient of velocity potentials Ψ.

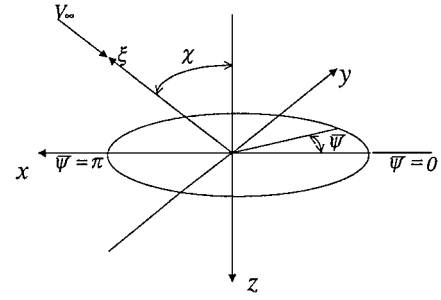

Fig. 1 Coordinate system.

New Formulation

Pressure Potentials and Velocity Potentials

To transform Eqs. (1) and (2) by a Galerkin method, it is required to expand the pressure potential Φ and the velocity potential Ψ in terms of a complete set of functions that satisfy Laplace's equation. In addition, they have to fulfill the boundary conditions for pressure in the case of Φ and for velocity in the case of Ψ.

The boundary conditions for pressure are given by a discontinuity across the rotor disk. The ellipsoidal coordinate system[5] has a discontinuity in ν across the rotor disk, and this allows representation of discontinuities across the rotor disk. An additional advantage of using an ellipsoidal coordinate system is that an analytical solution of Laplace's equation is known and can be expressed as

$$\Phi_n^{mc}(\nu, \eta, \bar{\psi}) = \bar{P}_n^m(\nu)\bar{Q}_n^m(i\eta)\cos(m\bar{\psi}) \tag{3}$$

$$\Phi_n^{ms}(\nu, \eta, \bar{\psi}) = \bar{P}_n^m(\nu)\bar{Q}_n^m(i\eta)\sin(m\bar{\psi}) \tag{4}$$

where $\bar{P}_n^m(\nu)$ and $\bar{Q}_n^m(i\eta)$ are normalized associated Legendre functions of first and second kind.[6]

Because $\bar{P}_n^m(\nu)$ with $n+m$ odd is an odd function of ν (as well as a function that satisfies Laplace's equation), Eqs. (3) and (4) can be used as the expansion functions for the pressure potentials. On the other hand, $\bar{P}_n^m(\nu)$ with $n+m$ even is an even function of ν, but its derivative with respect to z is an odd function of ν on the disk. Such functions can be used to represent mass sources at the rotor disk. Therefore, P can be written as a summation of terms that includes both pressure discontinuities and mass-sources terms. Additionally, it can be shown that the pressure potentials Φ_m^m result in velocity distributions with infinite kinetic energy.[7] Therefore, these are not included in the pressure expansion:

$$P = -\sum_{m=0}^{\infty}\sum_{n=m+1}^{\infty}\left[\tau_n^{mc}(\tau)\Phi_n^{mc} + \tau_n^{ms}(\tau)\Phi_n^{ms}\right] \tag{5}$$

The boundary conditions for the velocity field are that 1) the velocity field far away from the rotor is equal to zero and 2) there is a velocity discontinuity any place a vortex or vortex sheet exists in the flowfield. These discontinuities only exist at the rotor blades and within the rotor wake.

If the velocity field domain is limited to the infinite upper-half volume above the rotor disk (Fig. 2), the functions to be used in the velocity expansion need not fulfill any discontinuity conditions. Note that, in the case of perfectly edgewise flow, the wake is located on the rotor disk plane. Thus, no convergence of this methodology is expected on the trailing region off the rotor disk because the assumption for the velocity potentials is no longer valid in this region.

To satisfy strongly the upstream boundary condition for the velocity field at infinity, the velocity potentials are defined as

$$\Psi_n^{mc} = \int_\xi^\infty \Phi_n^{mc}\,\mathrm{d}\xi, \qquad \Psi_n^{ms} = \int_\xi^\infty \Phi_n^{ms}\,\mathrm{d}\xi$$

$$m = 0, 1, 2, \ldots, \infty, \qquad n = m, m+1, m+2, \ldots, \infty \tag{6}$$

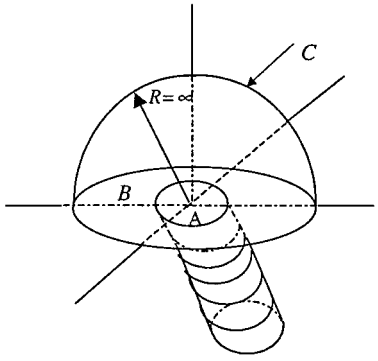

Fig. 2 Volume and area of integration.

This strongly ensures a zero velocity upstream. As ξ approaches infinity, Ψ_n^m approaches zero. The velocity $\boldsymbol{v}$ is taken as

$$\boldsymbol{v} = \sum_{m=0}^{\infty}\sum_{n=m}^{\infty}\left(\hat{a}_n^m(\tau)\nabla\,\Psi_n^{mc} + \hat{b}_n^m(\tau)\nabla\,\Psi_n^{ms}\right) \tag{7}$$

where Ψ_n^{mc} and Ψ_n^{ms} are defined by Eq. (6).

Substitution of Eqs. (5) and (7) into Eq. (1), allows Eq. (1) be written for cosine terms as

$$\sum_{m=0}^{\infty}\sum_{n=m}^{\infty}\left(\nabla\,\Psi_n^{mc}\frac{\mathrm{d}\hat{a}_n^m}{\mathrm{d}\tau} - \nabla\,\frac{\partial\Psi_n^{mc}}{\partial\xi}\hat{a}_n^m\right) = \sum_{m=0}^{\infty}\sum_{n=m+1}^{\infty}\nabla\,\Phi_n^{mc}\tau_n^{mc} \tag{8}$$

Only the cosine terms are listed because sine and cosine completely decouple. However, an identical set of equations can be written for the sine terms.

Galerkin Approach

To reduce Eq. (8) to a set of ordinary differential equations for the velocity coefficients in term of the pressure coefficients, a Galerkin approach is applied. In a Galerkin methodology, Eq. (8) is premultiplied by the gradient of each one of some test functions Λ integrated over the domain, and the integrals are set to zero. Additionally, the test functions are defined from the same set of functions used to expand the pressure potential Φ and the velocity potentials Ψ,

$$\Lambda_j^{rc} = \Phi_j^{rc}, \qquad \Lambda_j^{rs} = \Phi_j^{rs}$$
$$r = 0, 1, 2, \ldots, \infty, \qquad j = r, r+1, r+2, \ldots, \infty \tag{9}$$

The resultant integrals over the upper-half volume are reduced to integrals over the surface by applying the divergence theorem. The surface S can be subdivided into three areas: two of them are located on the rotor disk plane ($z=0$), s, and correspond to the on-disk area A and the off-disk area B, and the third one corresponds to the area on the dome C (Fig. 2).

The pressure potentials Φ_n^{mc}, velocity potentials Ψ_n^{mc}, and test functions Λ_j^{rc} are such that all of the integrals over the dome surface C become zero. Therefore, the surface of integration becomes the rotor disk plane ($z=0$), s, and the conservation of momentum equation becomes

$$\sum_{m=0}^{\infty}\sum_{n=m}^{\infty}\iint_s \Phi_j^{rc}\left[\frac{\partial}{\partial z}\left(\int_0^{\infty}\Phi_n^{mc}\,\mathrm{d}\xi\right)\frac{\mathrm{d}\hat{a}_n^m}{\mathrm{d}\tau} + \frac{\partial\Phi_n^{mc}}{\partial z}\hat{a}_n^m\right]\mathrm{d}s$$
$$= \sum_{m=0}^{\infty}\sum_{n=m+1}^{\infty}\iint_s \Phi_j^{rc}\frac{\partial\Phi_n^{mc}}{\partial z}\,\mathrm{d}s\,\tau_n^m$$
$$r = 0, 1, 2, \ldots, \infty, \qquad j = r, r+1, r+2, \ldots, \infty \tag{10}$$

or

$$\sum_{m=0}^{\infty}\sum_{n=m}^{\infty}\iint_s \frac{\partial\Phi_j^{rc}}{\partial z}\left(\int_0^{\infty}\Phi_n^{mc}\,\mathrm{d}\xi\frac{\mathrm{d}\hat{a}_n^m}{\mathrm{d}\tau} + \Phi_n^{mc}\hat{a}_n^m\right)\mathrm{d}s$$
$$= \sum_{m=0}^{\infty}\sum_{n=m+1}^{\infty}\iint_s \frac{\partial\Phi_j^{rc}}{\partial z}\Phi_n^{mc}\,\mathrm{d}s\,\tau_n^m$$
$$r = 0, 1, 2, \ldots, \infty, \qquad j = r, r+1, r+2, \ldots, \infty \tag{11}$$

Equations (10) and (11) constitute two different forms of the momentum equation. Each one is a set of ordinary differential equations for the velocity potential coefficients in terms of the pressure coefficients. From Eqs. (10) and (11), it is observed that, for these sets of functions, the application of the divergence theorem allows one to move the derivative with respect to the unit-outward normal direction, $\partial/\partial z$, from the velocity potentials Ψ_n^{mc} (or from the pressure potentials Φ_n^{mc}) to the test functions Λ_j^{rc}. At this point, note that the Φ_n^m with $n+m$ odd are zero on the $z=0$ plane off the disk B, whereas the z derivatives of Φ_n^m with $n+m$ even are zero on region B. Because of this, the divergence theorem can be utilized with appropriate choice of $\partial/\partial z$ position such that all terms are zero on region B. The result is a set of integrals that need only be evaluated on region A (on disk) for which they can be evaluated in closed form. The expression obtained after applying this procedure can be condensed in the following equation:

$$[\tilde{L}^c]\left\{\overset{*}{\hat{a}}{}_n^m\right\} + [D^c]\left\{\hat{a}_n^m\right\} = [D^c]\left\{\tau_n^{mc}\right\} \tag{12}$$

where each one of the elements of the $\tilde{L}^c$ and D^c matrices are known in closed form. The expressions are shown in Appendix A.

Equation (12) is valid for any skew angle χ, and the skew angle appears in the equation in the expressions for the wake influence coefficient matrix $\tilde{L}^c$. This equation can be partitioned into two row groups and two column groups such that $m+n$ (or $j+r$) is odd or $m+n$ (or $j+r$) is even. These matrices are organized in the following way:

$$\left[\begin{array}{c:c} \begin{bmatrix} j+r=\text{odd}, \\ n+m=\text{odd}\end{bmatrix} & \begin{bmatrix} j+r=\text{odd}, \\ n+m=\text{even}\end{bmatrix} \\ \hdashline \begin{bmatrix} j+r=\text{even}, \\ n+m=\text{odd}\end{bmatrix} & \begin{bmatrix} j+r=\text{even}, \\ n+m=\text{even}\end{bmatrix}\end{array}\right]\left\{\begin{array}{c}\{n+m=\text{odd}\}\\ \hdashline \{n+m=\text{even}\}\end{array}\right\} \tag{13}$$

If only odd terms are taken, this reduces to the Peters et al. model.[2]

If Eq. (12) is organized as suggested in Eq. (13), it can be partitioned as

$$\left[\begin{array}{c:c}[\tilde{L}^c]_{o,o} & [\tilde{L}^c]_{o,e}\\ \hdashline [\tilde{L}^c]_{e,o} & [\tilde{L}^c]_{e,e}\end{array}\right]\left\{\begin{array}{c}\left\{\overset{*}{\hat{a}}{}_n^m\right\}_o\\ \hdashline \left\{\overset{*}{\hat{a}}{}_n^m\right\}_e\end{array}\right\} + \left[\begin{array}{c:c}[D^c]_{o,o} & [D^c]_{o,e}\\ \hdashline [D^c]_{e,o} & [D^c]_{e,e}\end{array}\right]\left\{\begin{array}{c}\{\hat{a}_n^m\}_o\\ \hdashline \{\hat{a}_n^m\}_e\end{array}\right\}$$
$$= \left[\begin{array}{c:c}[D^c]_{o,o} & [D^c]_{o,e}\\ \hdashline [D^c]_{e,o} & [D^c]_{e,e}\end{array}\right]\left\{\begin{array}{c}\left\{\tau_n^m\right\}_o\\ \hdashline \left\{\tau_n^m\right\}_e\end{array}\right\} \tag{14}$$

Potential Function Expansions

The nondimensional pressure drop and mass flow added to the velocity field (both across the disk), and the velocity everywhere in the upper-half plane can be computed for the cosine terms as

$$\frac{\Delta p}{\rho V_\infty^2} = [P_{\text{lower}} - P_{\text{upper}}]_{\eta=0}$$
$$= 2\sum_{m=0}^{\infty}\sum_{n=m+1,m+3,\ldots}^{\infty}\bar{P}_n^m(\nu)\left(\tau_n^{mc}\right)_o\cos(m\bar{\psi}) \tag{15}$$

$$\frac{\Delta \dot{m}}{\rho V_\infty} = [P_{\text{lower}} + P_{\text{upper}}]_{\eta=0}$$

$$= 2\sum_{m=0}^{\infty}\sum_{n=m+2,m+4,\ldots}^{\infty} \bar{P}_n^m(\nu)\left(\tau_n^{mc}\right)_e \cos(m\bar{\psi}) \tag{16}$$

$$\boldsymbol{v} = \sum_{m=0}^{\infty}\sum_{n=m}^{\infty} \hat{a}_n^m \nabla \Psi_n^{mc} = \sum_{m=0}^{\infty}\sum_{n=m}^{\infty} \hat{a}_n^m \nabla \left(\int_{\xi}^{\infty} \Phi_n^{mc}\, \mathrm{d}\xi\right) \tag{17}$$

From Eq. (17), it is seen that, to compute the velocity field, it is required to compute the velocity potentials Ψ_n^m by numerical integration

$$\Psi_n^m = \int_{\xi}^{\infty} \Phi_n^{mc}\, \mathrm{d}\xi \tag{18}$$

To avoid numerical integration and to be able to express the velocity potentials in terms of potentials known everywhere in the flowfield, a change of variable from $\hat{a}_n^m$ to a_n^m is introduced

$$\left\{\hat{a}_n^m\right\}^T \left\{\Psi_n^{mc}\right\} = \left\{a_n^{mc}\right\}^T \left\{\sigma_n^m \Phi_{n+1}^{mc} + \varsigma_n^m \Phi_{n-1}^{mc}\right\} \tag{19}$$

The constants σ_n^m and ς_n^m are chosen such that the new velocity potential will give no singularities when gradients of it are taken. This results in

$$\sigma_n^m = 1\Big/K_n^m\sqrt{(2n+1)(2n+3)((n+1)^2-m^2)} \tag{20}$$

$$\varsigma_n^m = 1\Big/K_n^m\sqrt{(4n^2-1)(n^2-m^2)}, \qquad n \neq m \tag{21}$$

where

$$K_n^m = \left(\frac{\pi}{2}\right)^{(-1)^{n+m}} H_n^m \tag{22}$$

$$H_n^m = \frac{(n+m-1)!!(n-m-1)!!}{(n+m)!!(n-m)!!} \tag{23}$$

Equation (19) can be used to express the velocity potentials in axial flow.[5] If a Galerkin approach is applied to Eq. (19), the following relationship can be obtained:

$$\left\{\hat{a}_n^m\right\} = [\tilde{L}^c]^{-1}[M^c]\left\{a_n^m\right\} \tag{24}$$

where

$$\lfloor M^c \rfloor = \lfloor \tilde{L}^c \rfloor_{\chi=0} \tag{25}$$

and where $[\tilde{L}^c]$ is the same matrix as defined in Eq. (12) and in Appendix A.

If Eq. (19) is substituted into Eq. (17), it yields

$$v_z = \sum_{m=0}^{\infty}\sum_{n=m+1}^{\infty} a_n^m \nabla\left(\sigma_n^m \Phi_{n+1}^{mc} + \varsigma_n^m \Phi_{n-1}^{mc}\right) \tag{26}$$

Because

$$\frac{\partial\left(\sigma_n^m \Phi_{n+1}^{mc} + \varsigma_n^m \Phi_{n-1}^{mc}\right)}{\partial z} = \Phi_n^m, \qquad n > m \tag{27}$$

the axial component of the velocity is given by

$$v_z = \sum_{m=0}^{\infty}\sum_{n=m+1}^{\infty} a_n^m \Phi_n^{mc} \tag{28}$$

The other components of the velocity are given by the folllowing experssions:

$$v_r = \sum_{m=0}^{\infty}\sum_{n=m+1}^{\infty} \frac{\partial \Psi_n^{mc}}{\partial \bar{r}}$$

$$v_r = \frac{\bar{r}|_{z=0}}{\eta^2+\nu^2}\sum_{m=0}^{\infty}\sum_{n=m+1}^{\infty} a_n^m\left(-\nu\frac{\partial \Psi_n^{mc}}{\partial \nu} + \eta\frac{\partial \Psi_n^{mc}}{\partial \eta}\right) \tag{29}$$

$$v_{\bar{\psi}} = \frac{1}{\bar{r}}\sum_{m=0}^{\infty}\sum_{n=m+1}^{\infty} \frac{\partial \Psi_n^{mc}}{\partial \bar{\psi}} = -\frac{1}{\bar{r}}\sum_{m=0}^{\infty}\sum_{n=m+1}^{\infty} m a_n^m \Psi_n^{ms} \tag{30}$$

If Eq. (24) is substituted into Eq. (12), the set of ordinary differential equations for the velocity coefficients in terms of the pressure coefficients for skewed flow becomes

$$[M^c]\left\{\overset{*}{a}_n^m\right\} + [D^c][\tilde{L}^c]^{-1}[M^c]\left\{a_n^m\right\} = [D^c]\left\{\tau_n^{mc}\right\} \tag{31}$$

In axial flow, this equation becomes

$$[M^c]\left\{\overset{*}{a}_n^m\right\} + [D^c]\left\{a_n^m\right\} = [D^c]\left\{\tau_n^{mc}\right\} \tag{32}$$

which is the equation presented by Peters and Morillo.[5] Thus, the equation presented in previous work for axial flow is a particular case of Eq. (31) when $\chi = 0$.

As shown in Eq. (31), the inverse of $\tilde{L}^c$ needs to be computed to determine the induced velocities. Thus, the inversion properties of this matrix need to be analyzed. $\tilde{L}^c$ is well conditioned at any skew angle for the number of odd and even terms included in the solution being as high as 25 harmonics, and each harmonic includes terms with the highest power of $\bar{r}$ equal to the number of the corresponding harmonic. This is equivalent to saying that $\tilde{L}^c$ is a 364×364 matrix. This procedure to determine the number of radial terms is known as the table method.[6] When the number of harmonics is greater than 25, $\tilde{L}^c$ becomes ill conditioned. Because the $[\tilde{L}^c]_{o,o}$ partition is always well conditioned (equivalent to the inflow influence coefficient on the Peters–He model[3]), the conditioning problem of the complete $\tilde{L}^c$ can be eliminated by truncating the number of even terms included in the velocity and pressure potential expansions. If the truncation process eliminates all of the even terms the Peters–He model is obtained.

Results

Results will now be presented that show velocity fields as obtained by this new methodology. The complete velocity fields at $z = 0$ and $z = -\bar{r}$ are presented for pressure distributions as well as mass injection input distributions. Comparisons will also be made with an exact convolution solution in the frequency domain[7] (Appendix B) and with the Peters–He model.[3] Recall, however, that the Peters–He model, only gives results for the axial component on the disk for pressure inputs. No off-disk flow and no flow due to mass sources can be found by the Peters–He model.

The convergence of the results will be determined by comparing the exact results obtained with the convolution approach with the results obtained with the Galerkin approach. The error norm E between two distributions v_1 and v_2 is defined as

$$(E)^2 = \frac{\int_{r=r_o}^{r_f} (v_1 - v_2)^2\sqrt{1-r^2}r\, \mathrm{d}r}{\int_{r=r_o}^{r_f} v_1^2\sqrt{1-r^2}r\, \mathrm{d}r} \tag{33}$$

For the Galerkin approach, two errors can be defined. One for the on-disk region ($r_o = -1$ and $r_f = 1$), and one for the on/off-disk region ($r_o = -2$ and $r_f = 2$) at an azimuth angle $\bar{\psi}$.

In Figs. 3–9, the Galerkin approach includes 20 harmonics for the odd terms and 16 for the even terms. The number of radial function terms is obtained by applying the table method,[6] and the test functions do not include the Φ_r^r terms.[5] Also, unless otherwise noted, the velocities are computed for $\bar{\psi} = 0$–180 deg, a fore-to-aft slice.

Figures 3–5 show the results for the three velocity components in axial flow ($\chi = 0$). Figure 3 shows the frequency response for the first cyclic pressure distribution Φ_2^1 at the rotor disk plane ($z = 0$) and at a frequency $\omega = 7.3$. At this frequency, the Peters–He model[3] presents the maximum error compared with the exact solution (13.5%) (Ref. 5). Figure 3a shows the results for the axial component of the induced velocity. A 1% agreement between the Galerkin solution and the exact solution is observed on and off disk. On the other hand, the Peters–He model[3] introduces an error in the on-disk solution near the edge of the rotor. In Fig. 3b the result for the radial component of the induced velocity is shown. Again, excellent agreement between both solutions is observed in the in-phase as well as the out-of-phase response. [The induced velocity must be

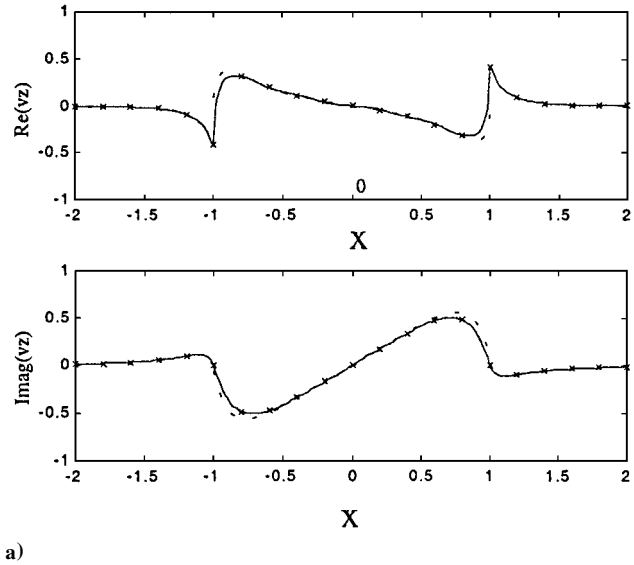

a)

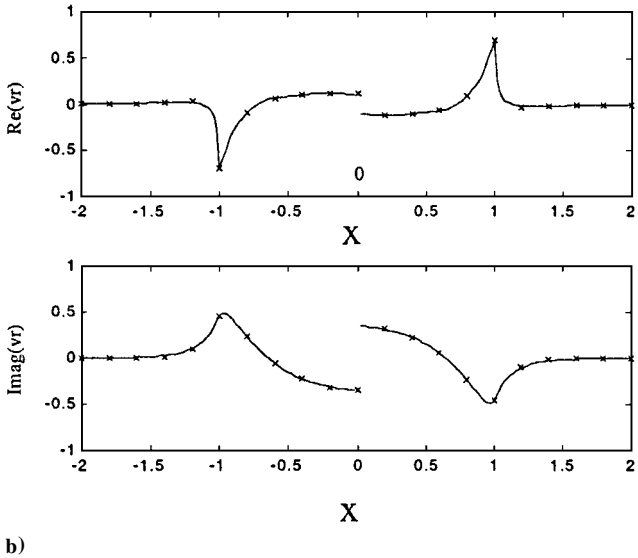

b)

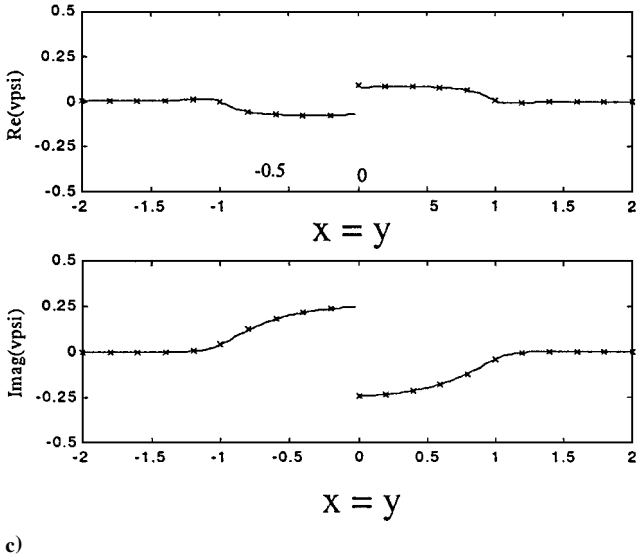

c)

Fig. 3 Frequency response $\omega = 7.3$, $P = \Phi_2^1$, and $\chi = 0$ deg: ×, convolution; ——, Peters–Morillo model[5]; and – – –, Peters–He model.[3]

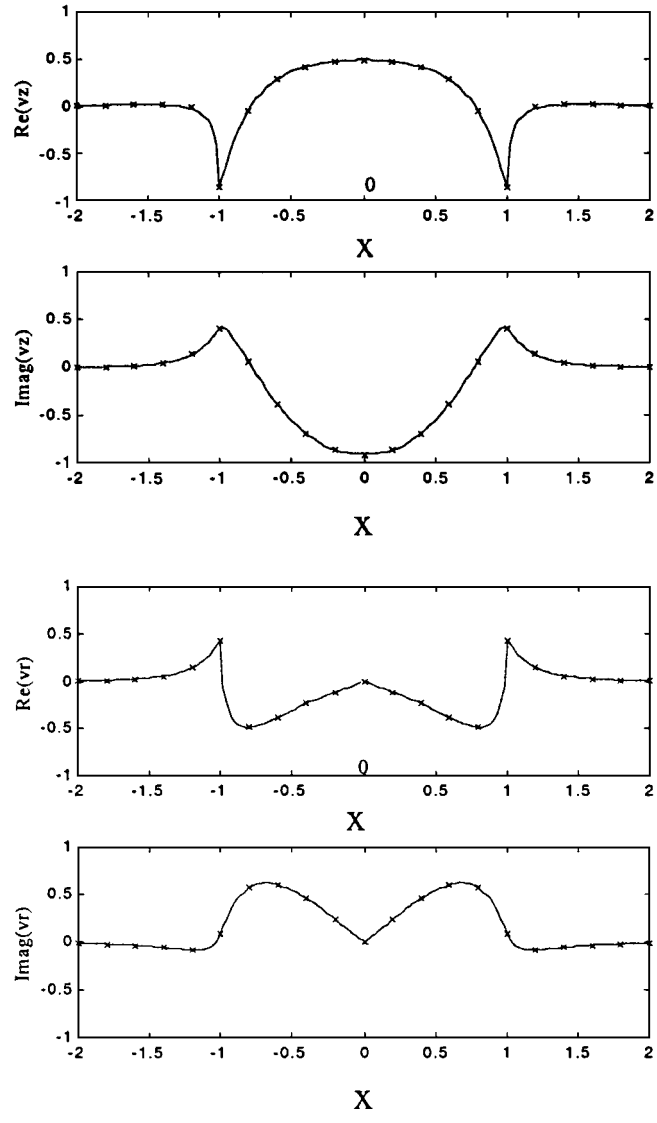

Fig. 4 Frequency response $\omega = 5$, $P = \Phi_2^0$, and $\chi = 0$ deg: ×, convolution and ——, Peters–Morillo model.[5]

continuous across the disk center. Therefore, v_r must change sign for a $\cos(\bar{\psi})$ input like Φ_2^1.]

Figure 3c shows the frequency response for the azimuthal component of the induced velocity. For this component, the induced velocity for any collective pressure or collective mass injection case ($m = 0$) is zero. This is also true for cyclic inputs ($m = 1$) at $\bar{\psi} =$ 0 or 180 deg. Therefore, in Fig. 3c the values are computed at $\bar{\psi} =$ 45–225 deg. Again, the Galerkin solution provides the exact solution both on and off the disk.

Figure 4 shows the axial and radial components of the induced velocity when the input is the first collective mass source distribution Φ_2^0 ($n + m =$ even) at a frequency $\omega = 5.0$. The convergence for mass flow is as excellent as is that for a pressure drop.

Next, attention is turned to computation of the velocity components not at the rotor disk plane but at one radius above the rotor disk ($z = -\bar{r}$). This is shown in Fig. 5 for the same pressure distribution, skew angle, and frequency as that of Fig. 3. Some important observations can be taken from Fig. 5 by comparing it with the response at the rotor disk plane (Fig. 3). First, the Galerkin solution matches the exact solution over the whole domain of the x values, as it does at $z = 0$. Second, the induced velocity above the rotor disk is considerably smaller than the one at the rotor disk.

In Figs. 6–9, the same pressure and mass source distributions are analyzed but for two different skew angles $\chi = 45$ and 75 deg. Figure 6 is for the first cyclic pressure distribution Φ_2^1 at a skew angle $\chi = 45$ deg. The Galerkin solution converges to the exact

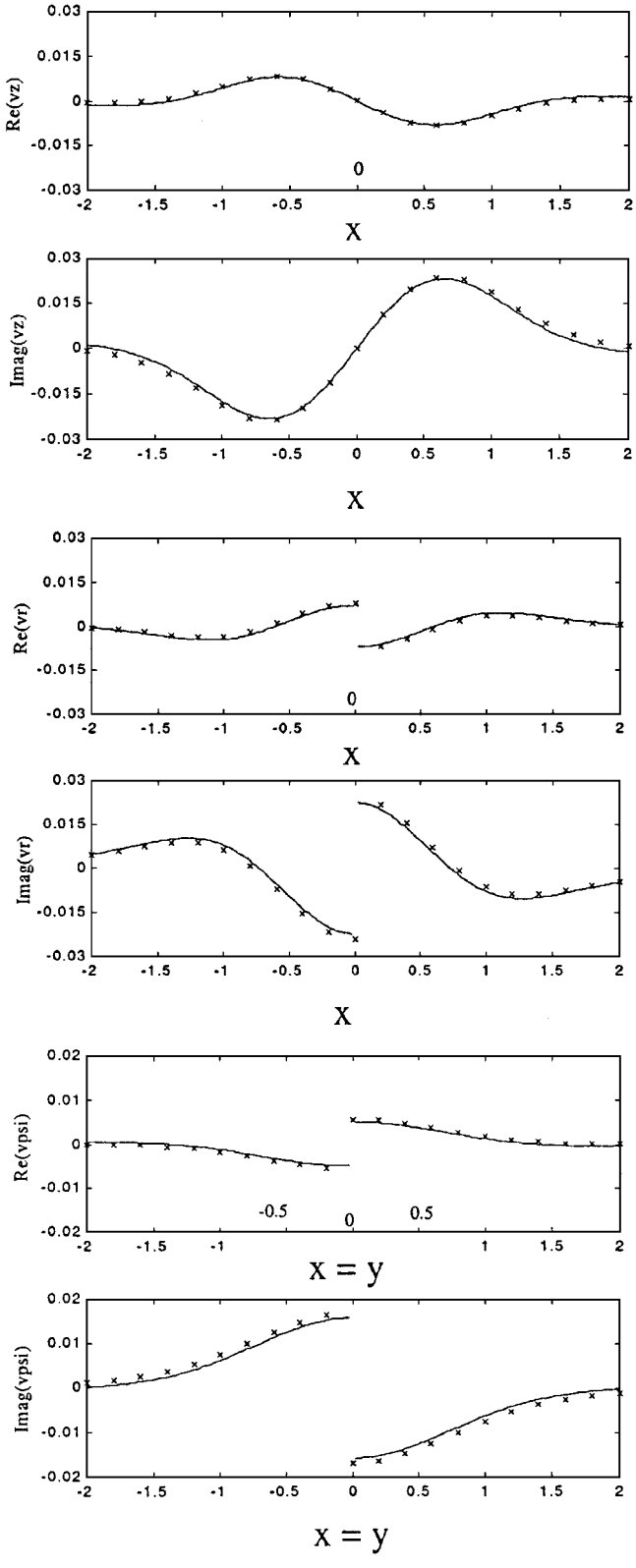

Fig. 5 Frequency response $\omega = 7.3$, $P = \Phi_2^1$, $\chi = 0$ deg, and $z = -1$: ×, convolution and ——, Peters–Morillo model.[5]

solution in-phase as well as the out-of-phase. The error in the on-disk region is 1.5% and for the entire region is 7.3%. The average error on the Peters–He model[3] is 9.7%, and it is largest in the region close to the edge. For a mass source input distribution Φ_2^0 (Fig. 7), the convergence toward the exact solution is excellent. The on-disk error is 1.5% and on the on/off disk is 6.9%. In both Figs. 6 and 7, the convergence of the methodology is slower on the trailing off-disk region for $x \leq -1.5$.

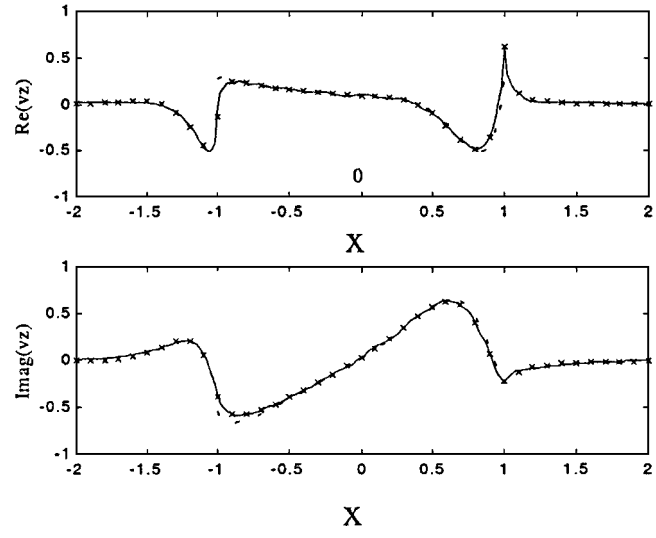

Fig. 6 Frequency response $\omega = 7.3$, $P = \Phi_2^1$, and $\chi = 45$ deg: ×, convolution; ——, Peters–Morillo model[5]; and – – –, Peters–He model.[3]

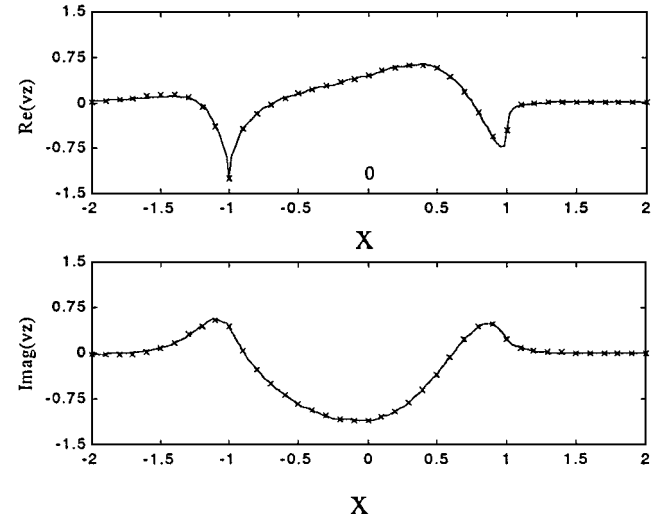

Fig. 7 Frequency response $\omega = 5$, $P = \Phi_2^0$, and $\chi = 45$ deg: ×, convolution and ——, Peters–Morillo model.[5]

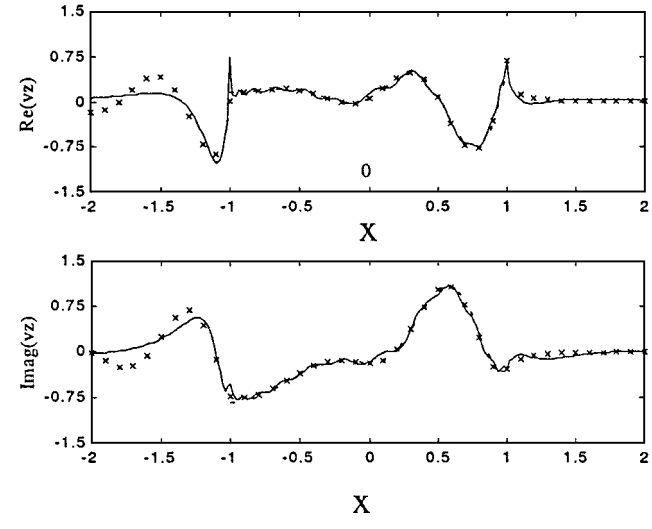

Fig. 8 Frequency response $\omega = 7.3$, $P = \Phi_2^1$, and $\chi = 75$ deg: ×, convolution; ——, Peters–Morillo model[5]; and – – –, Peters–He model.[3]

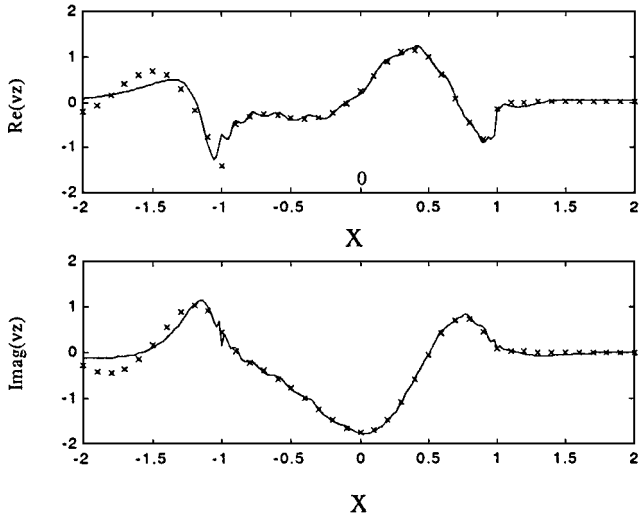

Fig. 9 Frequency response $\omega = 5$, $P = \Phi_2^0$, and $\chi = 75$ deg: ×, convolution and ——, Peters–Morillo model.[5]

Figures 8 and 9 are for a much steeper skew angle, $\chi = 75$ deg. The input in Fig. 8 is Φ_2^1. It is observed that, for the on-disk area, the Galerkin approach is converging toward the exact solution with an error of 6.5%. For the off-disk leading-edge region, the Galerkin approach gives a good correlation. For the off-disk trailing-edge region, as expected, the method is converging more slowly due to proximity to the wake The total on/off-disk error is 46.5%. In this case, the Peters–He model[3] is as accurate as the Galerkin approach (6.2%). Similar behavior is observed in Fig. 9. The on-disk error is 7.6% and the on/off-disk error is 39.1%. Note that for events very near the edge of the disk, the Peters–He[3] and Peters–Morrillo[5] results are indistinguishable in Figs. 3–8.

Conclusions

1) The conservation of mass and momentum equations (partial differential equations) are transformed to a set of ordinary differential equations in state-space form. This transformation is done by a Galerkin approach. In this Galerkin approach, test and trial functions are assumed to have the structure of the potential-flow functions utilized in the Peters–He model[3] but including terms with $n + m$ even as well as $n + m$ odd. These ordinary differential equations are written in matrix form, and they represent relations between the velocity coefficients and the pressure coefficients. The new methodology allows one to compute the complete velocity field, that is, all three components, everywhere in the volume above the rotor disk. Therefore, the flow off the disk can be computed, as well as the flow at a distance z above the disk.

2) All of the elements of the matrix formulations are developed in closed form, and they are functions of the skew angle χ. Therefore, this new formulation is still an extremely efficient model for preliminary design, real-time simulations, and dynamic eigenvalue analysis for aeroelasticity. Additionally, because the structure of previous inflow models is kept, it can be easily incorporated into the codes in which the Peters–He model[3] is actually used.

3) The equations are successfully applied in a frequency analysis for axial flow as well as for two different skew angles, $\chi = 45$ and 75 deg. They hold for pressure excitations ($n + m =$ odd) as well as mass source forcing functions ($n + m =$ even).

4) For axial flow, this new methodology gives the exact solution for all three components of the induced velocity on as well as off the rotor disk.

5) For skewed flows, $\chi = 45$ deg, the results for the axial component of the velocity on the disk show that this new methodology provides a more accurate value than the Peters–He model[3] for the on-disk values. In addition to that, it computes the velocity off disk, for the leading as well as the trailing edge. From the results for off-disk area close to the leading edge, the methodology provides the exact value, whereas for the area close to the trailing edge, the convergence of the methodology is slower.

6) For skewed flow close to perfectly edgewise flow, $\chi \geq 75$ deg, the Peters–He model[3] converges faster than the new model obtained by a Galerkin approach. On the off-disk region upstream from the leading edge, the new methodology converges to the exact solution.

Appendix A: Closed-Form Expressions

Mass matrix:

$$M_{jn}^{rm} = \frac{2}{\sqrt{H_n^m H_j^m}} \frac{(-1)^{(n+j-2m)/2}\sqrt{(2n+1)(2j+1)}}{(n+j)(n+j+2)[(n-j)^2-1]}$$

$$r = m, \qquad j + r = \text{odd}, \qquad n + m = \text{odd} \tag{A1}$$

$$M_{jn}^{rm} = \frac{1}{\sqrt{H_n^m H_j^r}\sqrt{(2n+1)(2j+1)}}$$

$$r = m, \qquad j = n \pm 1, \qquad j + r = \text{odd}, \qquad n + m = \text{even}$$

$$r = m, \qquad j = n \pm 1, \qquad j + r = \text{even}, \qquad n + m = \text{odd} \tag{A2}$$

$$M_{jn}^{rm} = \frac{8}{\pi^2\sqrt{H_n^m H_j^m}} \frac{(-1)^{(n+j-2m+2)/2}\sqrt{(2n+1)(2j+1)}}{(n+j)(n+j+2)[(n-j)^2-1]}$$

$$r = m, \qquad j + r = \text{even}, \qquad n + m = \text{even} \tag{A3}$$

$$M_{jn}^{rm} = 0, \qquad r \neq m \tag{A4}$$

Damping matrix:

$$D_{jn}^{rm} = \frac{1}{K_n^m}\delta_{jn}$$

$$r = m, \qquad j + r = \text{odd}, \qquad n + m = \text{odd}$$

$$r = m, \qquad j + r = \text{even}, \qquad n + m = \text{even} \tag{A5}$$

$$D_{jn}^{rm} = \frac{2}{\pi\sqrt{H_n^m H_j^m}} \frac{\sqrt{(2j+1)(2n+1)}}{(j+n+1)(j-n)}(-1)^{(j+3n-1)/2}$$

$$r = m, \qquad j + r = \text{odd}, \qquad n + m = \text{even}$$

$$r = m, \qquad j + r = \text{even}, \qquad n + m = \text{odd} \tag{A6}$$

$$D_{jn}^{rm} = 0, \qquad r \neq m \tag{A7}$$

Influence coefficient matrix:

$$\left(\tilde{L}_{jn}^{0m^c}\right) = \mathrm{X}^m\left(\Gamma_{jn}^{0m}\right) \tag{A8}$$

$$\left(\tilde{L}_{jn}^{rm^c}\right) = \left(\mathrm{X}^{|m-r|} + (-1)^l \mathrm{X}^{|m+r|}\right)\left(\Gamma_{jn}^{rm}\right) \tag{A9}$$

$$\left(\tilde{L}_{jn}^{rm^s}\right) = \left(\mathrm{X}^{|m-r|} - (-1)^l \mathrm{X}^{|m+r|}\right)\left(\Gamma_{jn}^{rm}\right) \tag{A10}$$

where

$$\mathrm{X} = \tan\left(\frac{\chi}{2}\right), \qquad l = \min(r, m) \tag{A11}$$

$$\Gamma_{jn}^{rm} = \frac{\text{sign}(r-m)}{\sqrt{K_n^m K_j^r}\sqrt{(2n+1)(2j+1)}}\delta_{j,n\pm 1}$$

$$r + m = \text{odd}, \qquad j + r = \text{odd}, \qquad n + m = \text{odd}$$

$$r + m = \text{odd}, \qquad j + r = \text{even}, \qquad n + m = \text{even} \tag{A12}$$

$$\Gamma_{jn}^{rm} = \frac{(-1)^{(n+j-2r)/2}(2)\sqrt{(2n+1)(2j+1)}}{\sqrt{H_n^m H_j^r}(n+j)(n+j+2)[(n-j)^2-1]}$$

$$r+m = \text{even}, \qquad j+r = \text{odd}, \qquad n+m = \text{odd} \quad \text{(A13)}$$

$$\Gamma_{jn}^{rm} = \frac{(-1)^{(n+j-2r+2)/2}(8)\sqrt{(2n+1)(2j+1)}}{\pi^2\sqrt{H_n^m H_j^r}(n+j)(n+j+2)[(n-j)^2-1]}$$

$$r+m = \text{even}, \qquad j+r = \text{even}, \qquad n+m = \text{even} \quad \text{(A14)}$$

$$\Gamma_{jn}^{rm} = \frac{(-1)^{(3n+j+2m-2r)/2}(4)\,\text{sign}(r-m)\sqrt{(2n+1)(2j+1)}}{\pi\sqrt{H_n^m H_j^r}(n+j)(n+j+2)[(n-j)^2-1]}$$

$$r+m = \text{odd}, \qquad j+r = \text{odd}, \qquad n+m = \text{even}$$

$$r+m = \text{odd}, \qquad j+r = \text{even}, \qquad n+m = \text{odd} \quad \text{(A15)}$$

$$\Gamma_{jn}^{rm} = \frac{1}{\sqrt{H_n^m H_j^r}\sqrt{(2n+1)(2j+1)}}\delta_{j,n\pm 1}$$

$$r+m = \text{even}, \qquad j+r = \text{odd}, \qquad n+m = \text{even}$$

$$r+m = \text{even}, \qquad j+r = \text{even}, \qquad n+m = \text{odd} \quad \text{(A16)}$$

$$K_n^m = \left(\frac{\pi}{2}\right)^{(-1)^{n+m}} H_n^m \quad \text{(A17)}$$

$$H_n^m = \frac{(n+m-1)!!(n-m-1)!!}{(n+m)!!(n-m)!!} \quad \text{(A18)}$$

Appendix B: Exact Solution

The exact solution for the complex velocity for a simple harmonic excitation

$$\bar{v}_i(x,y,z) = \bar{u}(x,y,z) + j\bar{w}(x,y,z), i = z, \bar{r}, \bar{\psi} \quad \text{(B1)}$$

can be obtained by a convolution integral,

$$\bar{u}(\xi_o) = \int_{+\infty}^{\xi_o} \cos[\omega(\xi_o - \xi)] G_{n_i}^m(\xi)\, d\xi \quad \text{(B2)}$$

$$\bar{w}(\xi_o) = \int_{+\infty}^{\xi_o} \sin[\omega(\xi_o - \xi)] G_{n_i}^m(\xi)\, d\xi \quad \text{(B3)}$$

where

$$G_{n_i}^m(\xi) = \begin{cases} \dfrac{\partial \Phi_n^{mc}}{\partial z}, & i = z \\ \dfrac{\partial \Phi_n^{mc}}{\partial \bar{r}}, & i = \bar{r} \\ \dfrac{1}{\bar{r}}\dfrac{\partial \Phi_n^{mc}}{\partial \bar{\psi}}, & i = \bar{\psi} \end{cases} \quad \text{(B4)}$$

Acknowledgment

This work was sponsored by The Boeing Company–Washington University Partnership and by the Army Research Office, Technical Monitor, Tom Doligalski.

References

[1]Pitt, D. M., and Peters, D. A., "Theoretical Prediction of Dynamic Inflow Derivatives," *Vertica*, Vol. 5, No. 1, 1981, pp. 21–34.

[2]Peters, D. A., He, C.-J., and Boyd, D. D., "A Finite-State Induced-Flow Model for Rotors in Hover and Forward Flight," *Journal of the American Helicopter Society*, Vol. 34, No. 4, 1989, pp. 5–17.

[3]Peters, D. A., and He, C.-J., "Correlation of Measured Induced Velocities with a Finite-State Wake Model," *Journal of the American Helicopter Society*, Vol. 36, No. 3, 1991, pp. 59–70.

[4]Xin, H., Prasad, J. V. R., Peters, D., Ibushi, N., and Nagashima, T., "Correlation of Experimental Measurements with a Finite-State Ground Effect Model," *Proceedings of the 56th Annual National Forum of the American Helicopter Society*, Virginia Beach, VA, May 2000, pp. 421–430.

[5]Peters, D. A., and Morillo, J. A., "Towards a Complete Dynamic Wake Model in Axial Flow," *Proceedings of the American Helicopter Society Aeromechanics Specialists' Meeting*, Atlanta, Nov. 2000.

[6]He, C.-J., "Development and Application of a Generalized Dynamic Wake Theory for Lifting Rotors," Ph.D. Dissertation, Georgia Inst. of Technology, School of Aerospace Engineering, Atlanta, July 1989.

[7]Morillo, J. A., "A Fully Three-Dimensional Unsteady Rotor Inflow Model from a Galerkin Approach," Ph.D. Dissertation, Dept. of Mechanical Engineering, Washington Univ., St. Louis, MO, Dec. 2001.